Physics – Uspekhi **54** (12) 1227 – 1242 (2011)

REVIEWS OF TOPICAL PROBLEMS PACS numbers: **61.05.–a**, **61.46.–w**, 64.70.P–, **64.75.–g**

Evolution of the structure of amorphous alloys

G E Abrosimova

DOI: 10.3367/UFNe.0181.201112b.1265

Contents

Abstract. This review addresses the current state of research on how amorphous alloys or metallic glasses evolve structurally from the initial amorphous to the final completely crystalline state. Structure transformations under heating, deformation, or irradiation conditions are considered. Particular attention is given to pre-crystallization processes. The stratification of a uniform amorphous phase into regions different in composition and/or in the type of short range order is described. The possibility is examined of whether completely or partially crystallized samples (single-phase, multi-phase, nanocrystalline, or those with surface-to-bulk difference) may have their structures modified to produce the required physical properties.

1. Introduction

In the amorphous state, metallic alloys were first produced in 1960 by a research group guided by Prof. P Duwez [1]. The very existence of a metallic alloy in a strange noncrystalline state was apprehended as a curious incident, and in one of the first publications Duwez, as he joked, placed his students in the first position on the list of the authors, 'concealing' himself behind them [1]. The work [1] is assumed to be the first publication that mentions amorphous alloys, or 'metallic glasses'. But, as a matter of fact, it was in 1959 that Miroshnichenko and Salli, who were working at that time in Dnepropetrovsk, USSR, demonstrated the possibility of producing metallic alloys in a noncrystalline state [2]. Be that as it may, it was the appearance of Ref. [1] that promoted an explosive increase in publications devoted to both the development of numerous methods of amorphization and investigations of the structure and properties of such strange objects. The high interest in metallic glasses remains, to a great extent, to date, and is related to their unusual structure and, in many cases, their unique properties and the possibility of producing now-popular nanocrystalline materials from amorphous alloys.

The properties of amorphous alloys differ from those of crystalline materials of the same composition [3]. Thus, for example, iron-based amorphous alloys have high strength. In alloys based on the elements of the iron subgroup (Fe, Co, Ni), the hardness (HV) can exceed 1000 units and the ultimate strength can be more than 4.0 GN m^{-2}. These values are greater than the maximum values of the strength and hardness of the metallic materials employed at present. The strength of wires made from some iron-based amorphous alloys is approximately 1.0 GN m^{-2} greater then that of so-called piano wire. The ratios of the yield stress to Young's modulus, σ/E, for amorphous alloys is 0.02–0.03, which is almost half the value corresponding to the theoretical strength ($\sigma/E = 0.05$). These ratios are significantly greater than those characteristic of the strongest metallic materials employed at present, for which σ/E is only $10^{-5}-10^{-2}$.

G E Abrosimova Institute of Solid State Physics,
Russian Academy of Sciences,
ul. Akademika Osip'yana 2, 142432 Chernogolovka, Moscow region,
Russian Federation
Tel. +7 (496) 522 46 85
Fax +7 (496) 522 81 60
E-mail: gea@issp.ac.ru

Received 7 April 2011, revised 10 June 2011
Uspekhi Fizicheskikh Nauk **181** (12) 1265 – 1281 (2011)
DOI: 10.3367/UFNr.0181.201112b.1265
Translated by S N Gorin; edited by M V Magnitskaya

[1] Reference [92] was erroneously missed in the Russian version. (*Editor's note added in English proof.*)

Among amorphous alloys, hard-magnetic and soft-magnetic, corrosion-resistant, and other materials are encountered.

From the viewpoint of industrial application, of greatest interest are the magnetic properties of amorphous alloys. It has been, for example, established that iron-based alloys have very good magnetic properties: small coercive force (0.5–1.0 A m^{-1}) and high saturation magnetization (exceeding 1.4 T). Even higher characteristics were obtained for $Co_{70}Fe_5Si_{15}B_{10}$ alloys [4] and for those of the Co–Fe–P–B system [5], which possess an almost zero magnetostriction. The soft magnetic properties of amorphous alloys can be improved by using relaxation annealing and annealing in a magnetic field. On the whole, the main characteristics of the soft magnetic alloys on the basis of iron, cobalt, and nickel are high values of the remanence and low magnetization-reversal losses; and high values of magnetic permeability at a high (at a large content of iron) or close-to-zero (at a large content of cobalt) magnetostriction. The magnetic properties can also be improved by the introduction of special alloying elements, in which case the magnitudes of the magnetic permeability can reach 120,000 [6].

Amorphous metallic alloys can be employed as a basis for the production of nanocrystalline materials. Owing to extremely small grain size, the structure of nanocrystalline materials is characterized by a large relative volume of grain and interphase boundaries, which can, to a significant extent, determine the various specific physical and chemical properties of the material. It has been established that many properties of nanocrystalline materials differ dramatically from those of both conventional polycrystals and amorphous alloys [7]. For example, nanocrystalline materials can have high strength and hardness, good plasticity and toughness, reduced elastic moduli, higher diffusion coefficients, a larger heat capacity and thermal-expansion coefficient, and better magnetic properties than conventional materials. Nanocrystalline alloys not only exhibit hysteretic magnetic properties on the level of the best crystalline alloys (such as permalloys) and amorphous alloys (cobalt-based alloys with nearly-zero magnetostriction), but also simultaneously have a high saturation induction, comparable with that of high-silicon electrical steels.

The materials of the other group — light nanocrystalline aluminum-based alloys — refer to high-strength materials [8–11]; the values of the yield stress in the aluminum-based alloys containing 6–15% transition metals (Fe or Ni) and a few percent rare-earth metals reach 1.6 GPa [12] at a sufficiently good plasticity. Note also that, while these values of strength are comparable with the strength of tool steel, the density of the aluminum-based alloys is less by a factor of approximately three.

Thus, the development of amorphous alloys proved to be an important step both in the investigation of nonequilibrium processes that occur in solids and in the designing of new materials, both amorphous and nanocrystalline. The phase transformations that occur, for instance, upon heating amorphous alloys exhibit a number of specific features. One such feature is the usual crystallization of the amorphous phase. Upon solidification, the transition from the liquid phase (melt) to the crystalline phase is accompanied by the liberation of heat, which leads to an increase in the sample temperature and, in the case of insufficiently rapid heat removal, can stop the process of crystallization. Heat is released upon the crystallization of an amorphous phase (which is in fact a frozen liquid) as well, but in this case the heating of the material surrounding the arising crystal will accelerate the process of crystallization, and at a sufficiently slow rate of heat removal can make this reaction self-accelerating (burst crystallization). The controlling of the parameters of crystallization in some cases makes it possible to create structures with large or small grain size, an equiaxed or substantially nonequiaxed shape of crystals, containing stable or metastable phases. Such structures, naturally, will possess different properties. However, for the production of a structure that has a required combination of physical properties, a clear understanding of processes occurring in amorphous materials under various treatments is necessary. Therefore, this review is devoted to the description of the evolution of the structure of amorphous alloys under heating, deformation, and other impacts.

2. Production of amorphous alloys

The most common method of production of metallic glasses is the rapid quenching of a melt onto a moving substrate, in which case the homogeneous metallic melt is cooled at a rate of 10^6 to 10^9 K s^{-1}, depending on the method of quenching. As a result of cooling at such rates, at room temperature a structure characteristic of a liquid is 'fixed' (becomes frozen), and the samples are noncrystalline.

With conventional slow cooling to the solidification temperature T_m, the liquid is crystallized. However, it is well known that upon rapid cooling the nucleation and growth of crystals is suppressed and the crystallization does not occur even at temperatures below T_m; instead, a supercooled liquid is formed. In addition, with decreasing temperature an increase occurs in the degree of supercooling, the rate of motion of atoms in the liquid drops significantly (correspondingly, the viscosity increases and the diffusion coefficient decreases), and, finally, the translational motion of atoms becomes very slow. In this case, the occurrence of crystallization and the formation of periodic atomic configurations is impossible; as a result, a solid is formed with the arrangement of atoms similar to that observed in a supercooled liquid. Such a nonequilibrium solid state is called a glassy state and the temperature at which the solidification occurs is called the glass transition temperature T_g. This temperature is frequently defined as the temperature at which the viscosity of the supercooled liquid reaches a value $\eta = 10^{12}$ P s.

The structure of the amorphous phase depends on the temperature of the melt before quenching, since the structure to be frozen is just that which is characteristic of a given temperature. Omitting details of the evolution of the melt structure with temperature, note the main thing: the structure of metallic glasses is amorphous: there are no signs of long-range order in it.

However, by no means can all the alloys be obtained in an amorphous state. Three criteria are usually considered to cause the diffusionless solidification of the alloy (without separation of its components) [13]:

• a thermodynamic criterion, which is based on the concept of a temperature T_0 (depending on the composition) at which the solid and liquid phases of the same composition have the same free energy;

• a morphological criterion, which determines at which velocity of the interface and at which magnitudes of the thermal gradients the interface is morphologically stable, i.e.

neither cells no dendrites are formed on it and the solidification is diffusionless;

• a thermal criterion, which requires an excessive supercooling corresponding to the degree of the supercooling of the liquid before the onset of the nucleation of the solid phase that is sufficient for the solidification of the entire melt even in the absence of the further removal of heat, without the liberation of the latent heat that causes heating of the sample to the equilibrium melting temperature.

One more important thing concerning the formation of an amorphous phase is the conditions necessary for the suppression of crystallization, namely, the kinetic and structural criteria for glass formation. The first criterion is related to the rate of cooling necessary to prevent the formation of any crystalline nuclei for purely kinetic considerations. The main condition for the formation of an amorphous phase is the impossibility of the formation of crystals in the process of rapid cooling. A number of calculations have been performed [14, 15] and the necessity that after cooling the volume fraction of the crystalline phase be no more than 10^{-6} was assumed to be a standard criterion for the formation of an amorphous state. The kinetic criterion works differently in different systems and depends, in particular, on the rates of diffusion of the alloy components. The structural criterion is determined by a whole group of factors, such as the relationship between the atomic radii of the alloy components, the enthalpy of the formation of atomic pairs, the electron concentration (Nagel–Tauc criterion [16]), the magnitude of the free volume, and, finally, the type of short-range order in the system.

The structure of the amorphous phase in metallic glasses has been described using various models. The first model was based on the dense random packing of hard spheres [17], which made it possible to successfully describe the atomic distribution functions in the amorphous structure. Later, this model was improved by the introduction of interatomic potentials (model of soft spheres), which permitted constructing pair atomic distribution functions [18] with more realistic values of the positions and intensities of the main part and of the shoulder of the second peak of the distribution function. Apart from the models of random packing of spheres and the microcrystalline model, which suggested that the structure consists of extremely fine crystals, a whole number of intermediate or combined variants has been discussed in the literature. All these models have one common feature, namely, the assumption of structure homogeneity. The real situation proved to be more complex; no one of the suggested models permitted an adequate description of the amorphous-structure evolution under various external exposures.

Later, investigations of the structure of metallic glasses were performed actively using both direct methods (X-ray diffraction, neutron diffraction, transmission and high-resolution electron microscopy) and indirect methods, for example, based on the study of the earlier stages of crystallization of the amorphous phase after various exposures. It should be noted that the second approach proved to be quite fruitful and made it possible to reveal a number of features related to structural transformations in amorphous phases.

3. Structural relaxation

It is important to note that the structure of an amorphous phase immediately after melt quenching is substantially nonequilibrium. In the 'initial' (as-quenched) state it is not metastable and usually relaxes to a state with a local minimum of free energy (metastable state). Reversible and irreversible structural relaxations are distinguished. The reversible relaxation is an initial fast process which is followed by a slower irreversible relaxation. The reversible structural relaxation is usually related to changes in the chemical short-range order; the irreversible relaxation is related to changes in the topological short-range order. The properties that change in an irreversible way upon relaxation are the volume, viscosity, diffusion mobility, and brittleness; the induced magnetic anisotropy can change reversibly; properties such as Young's modulus, heat capacity, coercive force, Curie temperature, and internal friction can behave, depending on the alloy composition, both reversibly and irreversibly [19]. The rate of relaxation depends also on the free volume; the smaller the free volume, the slower the structural rearrangements. The processes of structural relaxation have been studied in detail using the example of the alloy $Fe_{40}Ni_{40}P_{14}B_6$ [20, 21] and some others.

Since amorphous alloys are produced by quenching from the melt at rates of $10^6 - 10^9$ K s^{-1}, the structure of such 'frozen liquids' is nonequilibrium. At room temperature, quenched phases can be in different structural states, depending on the rate of cooling.

It is seen from Fig. 1 that the amorphous phases G_f and G_s, which arise with fast and slow cooling, respectively, differ in structure. The first has a high glass-transition temperature and a larger volume and the second has a low glass-transition temperature and a smaller volume. The increase in the quenching rate leads to an increase in the glass-transition temperature. Above this temperature, the substance is in the liquid state (supercooled liquid). Thus, the glass-transition temperature corresponds to the glass–liquid transformation. Upon heating, the phase G_f changes as shown in Fig. 1. First, at a temperature T_R, the structure passes from the state G_f into a more stable state G_s. It is this transition that is called structural relaxation. The unstable atomic configurations (arising at the moment of amorphization during quenching) pass into stable configurations via small atomic displace-

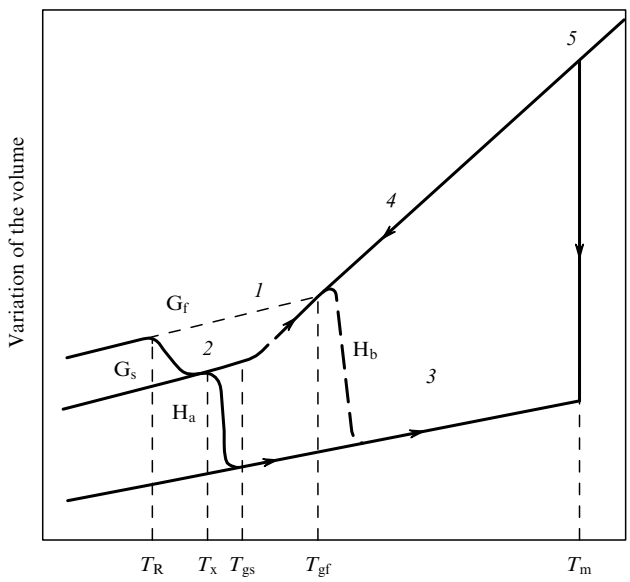

Figure 1. Variation of the volume upon heating of an amorphous phase: (*1*) rapidly cooled phase; (*2*) slowly cooled phase; (*3*) crystalline phase; (*4*) supercooled liquid; and (*5*) liquid.

ments; this results in a decrease in the free volume and, consequently, in the total volume as well. Note that the atomic displacements in the course of structural relaxation are less in magnitude than the interatomic spacings and occur in local regions.

Upon heating to sufficiently high temperatures, the possibility for atoms to become displaced to greater distances (via diffusion) appears, and the process of crystallization starts. In Figure 1 the onset of crystallization corresponds to the temperature T_x. It is seen that in this case the specific volume decreases sharply. In the majority of amorphous alloys, the crystallization starts below T_g (line H_a), but the amorphous state is still stable, since the crystallization terminates above the T_g temperature (line H_b).

The transformations that occur upon heating amorphous alloys can be roughly divided into two types: structural relaxation and crystallization. However, in real alloys the structural changes upon heating are quite varied and cannot be reduced to these two types. Egami [22], when considering structural relaxation, suggested that three types of structural changes in the amorphous phase should be taken into account:

(1) a significant decrease in free gaps available in the structure (decrease in the free volume);

(2) changes in the parameters of the geometrical (topological) short-range order; and

(3) changes in the parameters of the chemical short-range order.

Type-1 changes represent one of the processes of structural relaxation. The structural changes of types 2 and 3 are usually assumed to precede crystallization. For example, as was shown by Masumoto [23], prior to crystallization small crystalline clusters corresponding to the type-2 process arise, whereas the phase separation revealed by Chen [24] is assumed to correspond to the type-3 process.

Thus, since the processes that occur upon heating can be interlaced in a complex manner, it is difficult to separate them from one another. It is, however, important that the initial amorphous structure changes as a result of structural relaxation. Using various external exposures, the structure of the amorphous phase can be made substantially inhomogeneous. As external actions, processes such as heating, deformation, irradiation, or magnetic treatment can be used.

4. Methods of investigation of structures

Before we move to the discussion of examples concerning changes in structure under the effect of external factors, we should consider the most common techniques used for the detection and registration of structural changes, primarily, X-ray diffraction and small-angle X-ray and neutron scattering (SAXS and SANS, respectively).

One of the most informative, although rather labor-consuming, methods of the investigation of amorphous structures is the X-ray diffraction (XRD) technique. Figure 2 displays XRD patterns of a series of amorphous alloys of the Ni–Mo–B system taken in the region of the first diffuse halo. It is seen that the position of the diffuse maximum depends on the chemical composition and is related to the radius of the first coordination shell R_1 by the Ehrenfest relation [25]

$$2R_1 \sin\theta = 1.23\,\lambda\,, \tag{1}$$

where λ is the radiation wavelength, and θ is the diffraction angle.

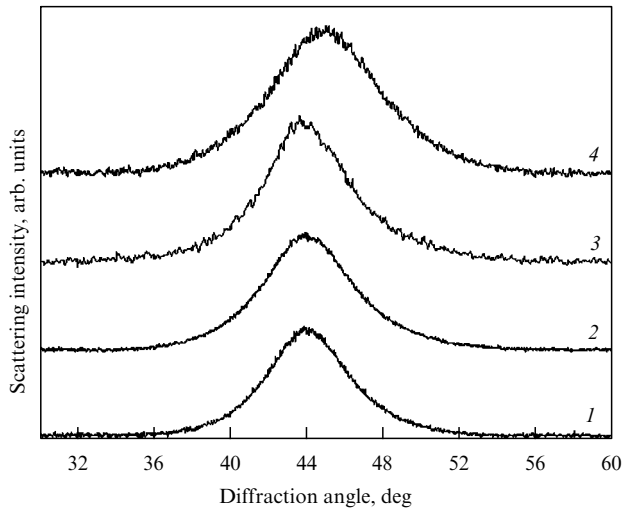

Figure 2. X-ray diffraction patterns of initial (as-quenched) amorphous alloys: (*1*) $(Ni_{70}Mo_{30})_{95}B_5$; (*2*) $(Ni_{70}Mo_{30})_{90}B_{10}$; (*3*) $(Ni_{65}Mo_{35})_{90}B_{10}$; and (*4*) $Ni_{70}Mo_{10}B_{20}$.

The radius of the first coordination shell R_1 is determined by the positions of the scattering-intensity maxima as follows:

$$R_1 = \frac{7.73}{S_{1\,\max}} = \frac{14.06}{S_{2\,\max}} = \frac{20.46}{S_{3\,\max}} \ldots, \tag{2}$$

where $S_{1\,\max} = 4\pi(\sin\theta/\lambda)$ is the wave vector corresponding to the ith (first, second, ...) maximum of the intensity curve, θ is the scattering angle, and λ is the radiation wavelength [20]. Since in the case of metallic glasses the first peak is substantially more intense than all subsequent ones, the radius of the first coordination shell is usually determined from its position.

A change in the position of the diffuse peak under the effect of some exposures indicates a change in the radius of the first coordination shell, i.e. a change in the composition of the amorphous phase. In those cases where the amorphous phase undergoes separation into two (or more) amorphous phases (regions with different compositions and/or different short-range order), the shape of the diffuse peak will be distorted — from the appearance of a shoulder to the separation into two (or more) maxima [26].

Some difficulties arise if the samples contain both amorphous and crystalline phases and if it is necessary to separate information related to only one of them. For multiphase samples containing different crystalline phases, a number of computer programs can be employed (e.g., PCW23 [27]) based on the comparison of the experimental and calculated diffraction patterns. To calculate the intensity of X-ray scattering, the following well-known formula is used [28]:

$$I = I_0 A(\mu,\theta)\, L(\theta)\, P(\theta)\, F^2(\mathrm{hkl})\, \exp(-2M)\, pV\,, \tag{3}$$

where I_0 is the intensity of the incident beam; $A(\mu,\theta)$ is the absorption factor; $L(\theta)\,P(\theta)$ is the combined (Lorentz and polarization) angular factor; $\exp(-2M)$ is the temperature factor; p is the multiplicity factor; V is the irradiated volume of the sample; and, finally, $F^2(\mathrm{hkl})$ is the structure factor, which depends on the positions of atoms in the crystal lattice. When using this method, it is naturally necessary to know the

atomic positions in the structure to be studied. In a crystalline structure, the positions of atoms in the lattice are usually known; therefore, such programs are used rather widely.

For the investigation of amorphous materials, this approach is unacceptable, since the atomic positions in such structures are unknown. The intensity of X-ray scattering by an amorphous phase is determined as follows [25]:

$$I(S) = NF^2(S)\left\{1 + \int_0^\infty 4\pi R^2 [\rho(R) - \rho_0] \frac{\sin(SR)}{SR} \, \mathrm{d}R\right\}, \tag{4}$$

where N is the full number of atoms per unit volume; $F(S)$ is the scattering amplitude; $\rho(R)$ is the number of atoms (per unit volume) that are at a distance R from the chosen atom; ρ_0 is the average number of atoms per unit volume; and S is the wave vector. As was noted above, to date there is no model that can adequately describe the positions of atoms in an amorphous structure. Therefore, the simulation of the scattering curve of an amorphous structure meets with serious difficulties.

In the analysis of XRD patterns of samples containing both amorphous and crystalline phases, the approach suggested by S Huang [29] is used most frequently, which is based on a comparison of the integrated intensities of the peaks from the amorphous and crystalline phases. In this case, the volume fraction of the crystalline phase, V_c, can be determined from the simple relation

$$V_c = \frac{I_c}{I_c + \alpha I_{am}}, \tag{5}$$

where I_c and I_{am} are the integrated intensities of the reflections from the crystalline and amorphous phases, respectively, and α is a constant. Naturally, it is necessary to take into account that in the case of mixed amorphous–crystalline samples there unavoidably occurs a mixing of the scattering from the amorphous phase with the diffraction from the crystalline phase, and the parameter α differs significantly in different systems [30, 31], but at comparable fractions of the amorphous and crystalline phases this approach is sufficiently correct [32].

One more actively used method in the investigation is the method of small-angle scattering of X-rays and neutrons. The most important feature of the method of small-angle scattering is the possibility of studying inhomogeneities in the structure of disordered systems, to which the metallic glasses refer, in fact. In an absolutely homogeneous medium small-angle scattering is absent and the scattering picture changes markedly upon the appearance of some inhomogeneities of the electron density in the structure. Investigations of the evolution of the pattern of small-angle scattering make it possible both to detect the appearance of inhomogeneities in the structure and to trace their variation (changes in the amount, dimensions, size distribution, relative change in the electron density compared to the matrix, etc.).

As is known [33], the intensity of X-ray scattering in the small-angle range is determined by the Guinier formula

$$I(q) = I_0 \exp\left(\frac{q^2 r_g^2}{3}\right), \tag{6}$$

where $q = (4\pi/\lambda)\sin(\theta/2)$ is the scattering wave vector; λ is the radiation wavelength; θ is the scattering angle of the radiation; and r_g is the radius of gyration. By constructing Guinier plots of the dependence of $\ln I(q)$ on q^2, the dimension and shape of the scattering particles can be determined from the slope of the straight line $r_g^2 \sim \ln(q)/q^2$. For an analysis of the small-angle scattering curves, the analysis of invariants is employed, in particular, the so-called Porod invariant

$$Q = \int_0^\infty q^2 I(q) \, \mathrm{d}q = 2\pi^2 \int_V \rho^2(\mathbf{r}) \, \mathrm{d}\mathbf{r}, \tag{7}$$

which is proportional to the square of the contrast of the particle $\pi(\mathbf{r})$ relative to the matrix (to the difference in the electron density). Under the conditions of a uniform distribution of particles, their volume in the sample can also be determined. Therefore, the application of the method of small-angle scattering makes it possible to analyze the structure of amorphous phases.

Thus, the evolution of the structure of an amorphous phase can be studied by the analysis of X-ray scattering curves.

And, undoubtedly, an important method for the investigation of the evolution of the structure of amorphous alloys is transmission electron microscopy (TEM), and especially high-resolution electron microscopy (HREM).

5. Evolution of the structure of amorphous phases under the effect of external factors

In connection with the above, various cases of the evolution of the structure of amorphous alloys in the amorphous state can be considered.

5.1 Evolution of the structure upon heat treatment

Upon heating, the amorphous alloys crystallize, but sometimes the crystallization is preceded by the separation of the amorphous phase into regions with different chemical compositions and different short-range orders, i.e., the formation of two or more amorphous phases occurs. These phases, as a rule, do not have distinct interfaces and upon transformation can manifest themselves as features characteristic of spinodal decomposition [34]. It has been shown when studying the structure of Pd–Au–Si alloys [35] that the phase separation processes depend on the chemical composition, and in this system the tendency to separation increases with increasing gold concentration. The authors of [35] revealed that in the alloy of composition $Pd_{0.8}Au_{0.035}Si_{0.165}$ a separation of the amorphous phase first occurs by the mechanism of nucleation and growth and later, upon crystallization, an fcc phase distributed in the amorphous phase (primary crystallization) is formed. The alloy of composition $Pd_{0.74}Au_{0.08}Si_{0.18}$ after separation crystallizes with the formation of two crystalline phases, which are formed one after another as follows:

$Pd_{0.82}Si_{0.18}$:

glass $\rightarrow T_g \rightarrow$ melt $\rightarrow$ homogeneous fcc solid solution;

$Pd_{0.8}Au_{0.035}Si_{0.165}$:

glass $\rightarrow T_g \rightarrow$ melt $\rightarrow$ phase separation $\rightarrow$ crystalline phase + melt $\rightarrow$ second crystalline phase;

$Pd_{0.74}Au_{0.08}Si_{0.18}$:

glass $\rightarrow T_g \rightarrow$ melt $\rightarrow$ phase separation $\rightarrow$ two liquid phases $\rightarrow$ two crystalline phases.

The authors of [35] also concluded that the decomposition, at least at the early stages, is spinodal with a length of the concentration wave of about 20 nm.

As examples of the observation of changes in the structure upon the heat treatment of amorphous phases, several studies can be mentioned. Thus, in the Pd–Au–Si alloy the initial amorphous phase was homogeneous, but after annealing at 400 °C phase separation into regions with different elemental compositions was observed [35]. In the $(Mo_{0.6}Ru_{0.4})_{100-x}B_x$ alloy [36], it was revealed that chemical segregation is developed already prior to the onset of crystallization; in [37] it was shown that in the alloy of composition $Fe_{67}Co_{18}B_{14}Si_1$ the initial amorphous phase was homogeneous, but after heating to 400–600 K regions enriched with boron and Fe–Co regions were formed, i.e., regions with different types of short-range order appeared. The short-range order in the amorphous phase naturally depends on the chemical composition of the alloy; its changes depending on the composition have been studied by a number of authors. For example, in [38] the changes in the structure of the amorphous alloy $(Zr_{0.667}Ni_{0.333})_{1-x}B_x$ were studied while the boron concentration changed from 0 to 25 at. %, and it was shown that at $x \approx 0.05$ a change occurred in the type of short-range order.

The evolution of the structure of an amorphous phase depends on temperature. Heating and annealing of metallic glasses can be implemented in two different temperature regions: above and below the glass transition temperature T_g. Above T_g, the amorphous phase is in the state of a supercooled liquid; below T_g, it is in the amorphous state proper. It is known that with the passage through the glass transition temperature T_g many properties of the material, e.g., the viscosity, enthalpy, heat capacity, and specific volume, change sharply [6], which leads to substantial differences in the process of diffusional mass transfer in these temperature ranges and, in turn, to changes in the structure.

Therefore, of most interest, in our opinion, is a comparison of structural changes in one and the same alloy occurring above and below the glass transition temperature. For comparison, we consider nickel-based alloys Ni–Mo–P and Ni–Mo–B.

5.1.1 Amorphous alloy $Ni_{70}Mo_{10}P_{20}$. The glass transition temperature of this alloy ($T_g = 430$ °C at the rate of heating of the sample of 20 K min^{-1}) is lower than the crystallization temperature ($T_x = 457$ °C) [38], which makes it possible to study changes in the structure both in the state of a supercooled liquid (above T_g) and in the amorphous state (below T_g).

Heating to above the glass transition temperature leads to noticeable changes in the structure of the amorphous phase. Figures 3 and 4 display electron micrographs of the structure of the initial sample (see Fig. 3) and of the sample annealed at a temperature above T_g (see Fig. 4) [39]. The electron-microscopic investigations of foils prepared under identical conditions reveal in the annealed sample, in contrast to the initial one, a distinctly pronounced spotty contrast.

Figure 5 demonstrates X-ray diffraction patterns of the initial samples and samples annealed at above T_g. The position of the diffuse maximum of the initial amorphous sample corresponds to $d = 0.205$ nm ($S = 4.88$ nm^{-1}). After annealing, the shape of the diffuse peak becomes distorted. An analysis of the diffraction pattern showed that the peak observed can be described by two Gaussians, although, of course, the observed diffraction pattern can better be described by a greater number of Gaussians; i.e., the structure of the sample can be characterized by a whole number of first coordination shells with a continuously changing radius. When analyzing the structure of an amorphous alloy using the method of selected-area electron diffraction (SAED), it has been established that the scattering vector corresponding to the maximum intensity of the diffuse halo obtained from the amorphous phase changes when going

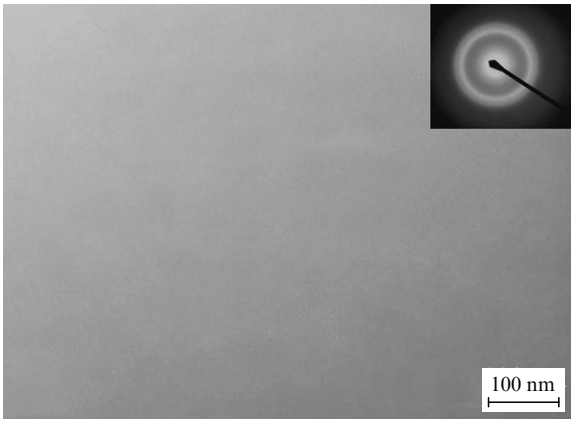

Figure 3. Structure of the initial amorphous sample $Ni_{70}Mo_{10}P_{20}$.

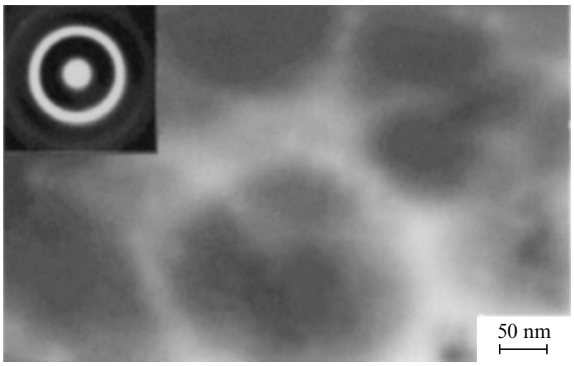

Figure 4. Structure of a sample of the $Ni_{70}Mo_{10}P_{20}$ alloy annealed at a temperature above T_g.

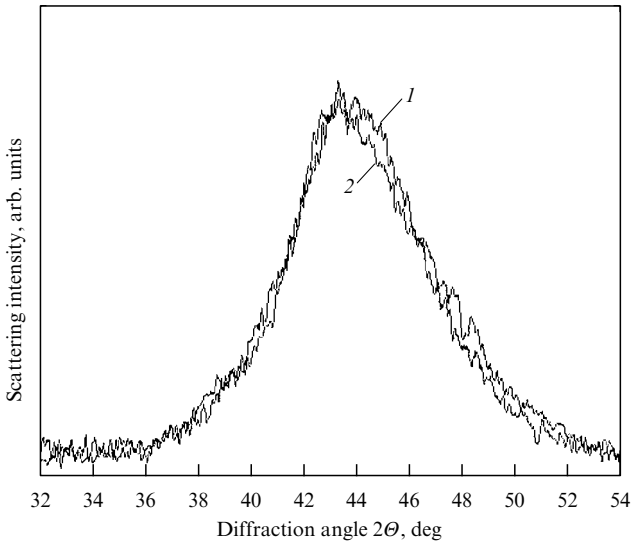

Figure 5. X-ray diffraction patterns of samples of the $Ni_{70}Mo_{10}P_{20}$ alloy: (*1*) initial and (*2*) annealed above T_g.

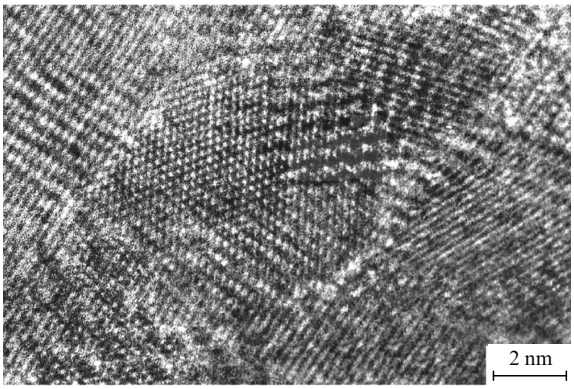

Figure 6. Structure of a sample of the $Ni_{70}Mo_{10}P_{20}$ alloy crystallized above T_g.

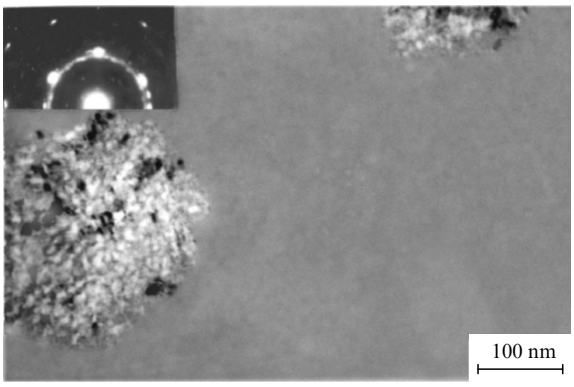

Figure 7. Structure of a sample of the $Ni_{70}Mo_{10}P_{20}$ alloy crystallized below T_g.

from one region of the sample to another. The maximum change in the scattering vector S ($S = 2\sin\theta/\lambda$, where θ is the scattering angle, and λ is the wavelength) was 0.1 nm^{-1}.

Thus, the observed regions of the spotty contrast and the matrix are described by different scattering vectors; this indicates that the short-range order in bright and dark regions is different.

Upon further heating, the crystallization starts at sites which look like lighter regions in micrographs. At these sites crystals (20–30 nm in size) of the fcc solid solution of Mo in Ni are formed, which frequently directly contact each other (Fig. 6).

If the heat treatment is performed below the glass-transition temperature, no changes in the structure of the amorphous phase are observed. The structure of a sample annealed at 400 °C (i.e., below T_g) for 1 h contains an amorphous phase and crystalline eutectic colonies consisting of two phases (Fig. 7). As is seen from Fig. 7, the amorphous matrix in the micrograph has a uniform contrast without any features. Upon the crystallization, as was said above, eutectic colonies are formed and the structure differs fundamentally from that observed above the glass-transition temperature.

Thus, above T_g, processes occur in the amorphous phase that lead to the appearance of regions about 100 nm in size, which have different contrasts in electron-microscopic images. The composition of 'bright' regions corresponds to the solid solution of Mo in Ni and, although several crystals are formed here, no intergrain regions of the amorphous matrix are observed, and the nanograins are in the direct contact with each other. It is obvious that these regions crystallize via the polymorphic mechanism, i.e., without a change in the chemical composition. Estimates of the composition of the solid solution performed on the basis of the magnitudes of the lattice parameter of the fcc phase in terms of the Vegard law showed that the content of molybdenum in the solid solution is $\sim$ 12 at. %. This value corresponds to the equilibrium solubility of Mo in Ni at the annealing temperature.

Upon crystallization below the glass-transition temperature, the mechanism of crystallization is different; namely, a eutectic crystallization occurs with the formation of colonies. In this case, the redistribution of the components prior to the start of crystallization is only insignificant, if it exists at all.

Thus, above and below the glass-transition temperature the structure of the amorphous phase upon heating changes differently, which leads to the formation of different crystal structures and, naturally, to different physical properties.

5.1.2 Amorphous alloy $Ni_{70}Mo_{10}B_{20}$ [40]. In this alloy the glass-transition temperature is also lower than the temperature of crystallization. When heating the amorphous alloy to above T_g, an increase in the half-width of the diffuse maximum in the X-ray diffraction patterns occurs. This change in the diffraction pattern is analogous to the above-described change in the diffraction pattern of the $Ni_{70}Mo_{10}P_{20}$ alloy. In the alloy with phosphorus, the process of phase separation manifested itself in an increase in the half-width of the diffuse maximum, which distorted with time; this was due to the formation of amorphous regions with different concentrations of components, which subsequently were crystallized with the formation of different phases.

In the $Ni_{70}Mo_{10}B_{20}$ alloy, the change in the diffraction pattern is also due to the appearance of regions of different chemical compositions. In this case, the observed diffuse maximum represents a superposition of several closely spaced diffuse peaks. In this alloy a concentration redistribution of the components occurs with the formation of regions enriched in and depleted of molybdenum (a redistribution of boron cannot lead to such a noticeable change in the half-width of the peak). Thus, prior to the start of crystallization the amorphous phase is inhomogeneous and consists of regions with increased and decreased concentrations of molybdenum (and, possibly, of boron).

The crystallization of the alloy at temperature above T_g leads to the simultaneous formation of three crystalline phases, namely, two fcc phases with the lattice parameters 0.3597 and 0.3541 nm, and an orthorhombic phase Ni_3B (Fig. 8). The fcc phases are Ni and a solid solution of Mo in nickel (Ni(Mo)). According to the results of the analysis by the method of energy-dispersive spectroscopy (EDS) in the transmission geometry, the composition of the solid solution corresponds to $Ni_{85}Mo_{15}$. With the occurrence of crystallization, the lattice parameter of this phase decreases somewhat, which is related to a decrease in the concentration of molybdenum in the nickel lattice.

During crystallization, all three phases are formed almost simultaneously. The sizes of crystallites do not exceed 50 nm. Figures 9 and 10 display HREM images of Ni nanocrystals and of the solid solution of Mo in Ni (Ni(Mo)) formed above the glass-transition temperature.

It is seen that each nanocrystal is surrounded by an amorphous matrix. TEM and HREM investigations of the structure showed that all three phases form independently of

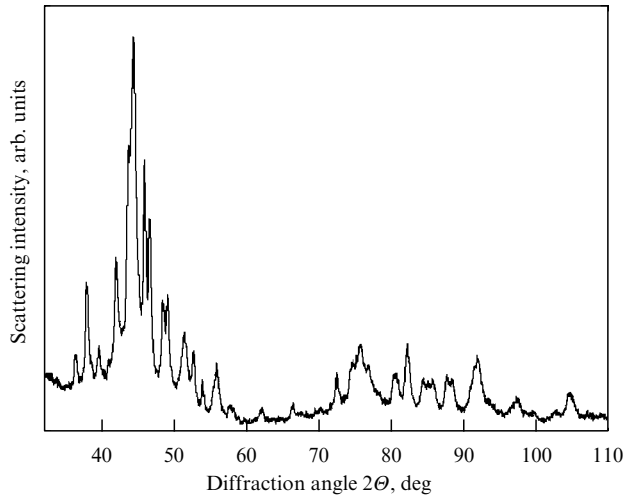

Figure 8. X-ray diffraction pattern of the $Ni_{70}Mo_{10}B_{20}$ alloy after annealing at 500 °C.

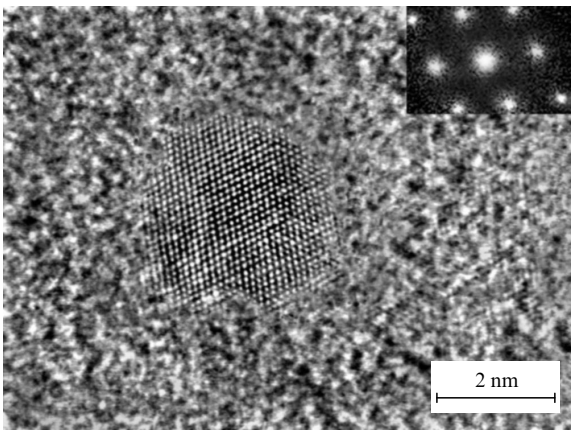

Figure 9. HREM image of Ni nanocrystal formed in the $Ni_{70}Mo_{10}B_{20}$ alloy at a temperature above T_g.

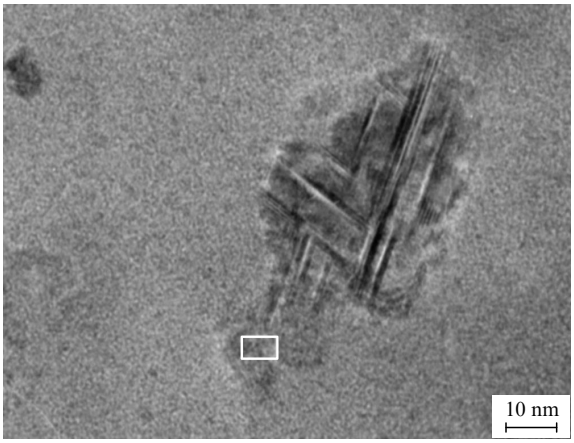

Figure 10. HREM image of a nanocrystal of the molybdenum solid solution in nickel Ni(Mo) formed in the $Ni_{70}Mo_{10}B_{20}$ alloy at a temperature above T_g.

one another. It is natural to suppose that the formation of each crystalline phase occurs in 'its own' concentration region; i.e., the formation of crystalline phases in each concentration region can occur via the polymorphic mechanism without a change in the chemical composition. Such a

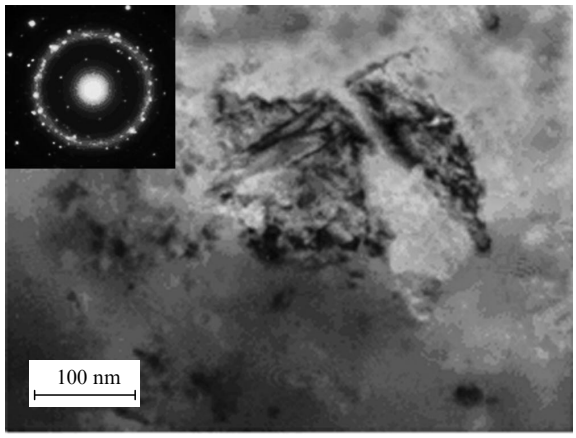

Figure 11. Electron micrograph of the structure of a sample of the amorphous alloy $Ni_{70}Mo_{10}B_{20}$ after 2 h annealing at a temperature of 733 K (below T_g).

mechanism of crystallization is caused by changes in the structure of the amorphous phase preceding crystallization and ensuring the formation of amorphous regions with a 'necessary' compositional ordering.

Below the glass-transition temperature, no phase separation preceding the crystallization is observed; the crystallization has a clearly pronounced eutectic character. The structure formed upon crystallization below the glass-transition temperature is shown in Fig. 11.

Thus, in the $Ni_{70}Mo_{10}B_{20}$ alloy, just as in the $Ni_{70}Mo_{10}P_{20}$ alloy, the structures formed at temperatures above and below T_g differ significantly.

Results indicating the development of inhomogeneities in the amorphous matrix have also been obtained through investigations of amorphous alloys by the SAXS method. Upon annealing, the intensity of small-angle scattering in the amorphous alloy $Fe_{90}Zr_{10}$ was found to grow significantly; during annealing at 653 K for 10 min, the size of inhomogeneous regions increased from 6 to 12 Å [41]. A noticeable increase in the intensity of small-angle scattering upon heating prior to the onset of crystallization was also revealed in this alloy in [42, 43]. The growth of intensity of small-angle scattering within the amorphous state was observed in Fe–P–C, Fe–B, Pd–Au–Si [44], and other alloys; in the amorphous Cu–Ti and Ni–Y alloys, small-angle scattering within the amorphous state was revealed for compositions that did not correspond to crystalline phases fixed in the phase diagrams of these alloys. In Ref. [45], no small-angle scattering was revealed in those cases where the composition of the amorphous phase corresponded to the composition of precipitated crystalline phases. The intensity of small-angle scattering increases with increasing temperature or annealing time. In all cases, the growth of intensity was caused by the formation of regions of inhomogeneities of the electron density, i.e., of regions with a chemical composition different from that of the matrix and/or different short-range order (regions of an amorphous phase of a different composition).

The use of only one method of small-angle scattering does not make it possible to determine the nature of regions of electron-density inhomogeneities; however, sometimes this can be performed by additionally using the HREM technique. Thus, in [46] it was shown by the simultaneous use of these two methods for the investigation of Fe–B amorphous

alloys that the appearance of small-angle scattering is related to the formation in the amorphous matrix of regions with a short-range order different from that characteristic of the matrix, namely, of regions that are nuclei of the Fe_3B phase which arises upon subsequent crystallization.

The changes in the structure of the amorphous phase under heat treatment are by no means necessarily reduced to phase separation. Under certain conditions, the change in the temperature can lead to a change in the type of short-range order [47, 48]. Thus, for example, in Fe–B amorphous alloys the short-range order in the amorphous phase can change with temperature from the type of packing characteristic of the orthorhombic boride Fe_3B (space group Pnma) to the type of packing inherent in the tetragonal boride Fe_3B (space group $P4_2/n$). Upon subsequent crystallization, the arising boride will be of that type which corresponds to the short-range order of the amorphous phase before the crystallization.

5.2 Evolution of the structure upon deformation

The structure of an amorphous phase can change markedly not only upon heating but also under the effect of deformation. The question of the possible variation of the structure under the impact of deformation emerged virtually at the very beginning of investigations of amorphous alloys. As an example, the review by C A Pampillo [49] can be mentioned, in which the deformation via homogeneous and inhomogeneous flow, the processes of fracture, and the effects of temperature and composition of amorphous metallic alloys on these processes were considered. Thus, for instance in the investigation of rolled strips of the $Pd_{80}Si_{20}$ alloy a shift of the position of the first peak of the structure factor toward smaller angles was observed [23]. However, no special investigations of structures were performed at that time. Nevertheless, one important fact should be noted, which was established almost at once in the investigations of the mechanical properties of amorphous alloys: at low temperatures and moderate loads, the plastic deformation is strongly localized and, in fact, occurs in narrow zones — shear bands — and does not virtually involve the main part of the amorphous phase. In these bands, the structure should naturally be changed.

In the recent years, a series of interesting studies devoted to studying the evolution of the structure directly in the process of deformation of zirconium-based amorphous alloys have appeared. The structural investigations were performed using a synchrotron X-ray source under tensile loading in situ, which made it possible to reveal structural changes occurring upon elastic deformation [50–52]. The authors of these works showed that in the absence of plastic deformation the tensile stress leads to changes in the interatomic spacings in the amorphous structure, and that these changes depend on the orientation of the applied stress. The zirconium-based amorphous alloys are brittle and virtually do not undergo plastic deformation; therefore, in these studies only the field of elastic deformation was considered. At the same time, it would be of interest to establish whether or not these changes are retained after the removal of stress and whether or not they exist upon plastic deformation. We performed such investigations on the amorphous alloy $Pd_{40}Ni_{40}P_{20}$. As the method of deformation, we used multiple rolling, and the investigations of the structure of deformed samples were performed both along and across the rolling direction [53].

As a result of the investigations performed, we revealed that, in contrast to the initial amorphous samples, the structure of the samples after deformation became anisotropic. Figure 12 shows an X-ray diffraction pattern of a sample after rolling to a reduction of 38%. Apart from the diffuse curves of scattering from the amorphous sample, the XRD pattern contains a peak from the silicon substrate ($2\theta = 33.15°$; reflection (111)), which can be used as a reference mark in the analysis. The identical positions of the reference mark indicate the identical position of the samples during the X-ray exposure (the absence of a shift from the focusing center). It is seen that the diffuse maxima from the sample, which were obtained for different mutual orientations of the X-ray beam and the deformation direction, are shifted relative to each other. These X-ray diffraction patterns were used to determine the shortest interatomic distances; it has been established that after deformation the interatomic spacings along the rolling direction increase, whereas in the transverse direction they remain virtually unaltered. With time, this effect was found to decrease. Thus, the structure of the amorphous phase changes in the process of deformation.

As was noted above, the effect of elastic tensile deformation on the structure of metallic glasses was studied using a series of zirconium-based alloys in [50–52]. The authors of these studies observed differences in the position of the first

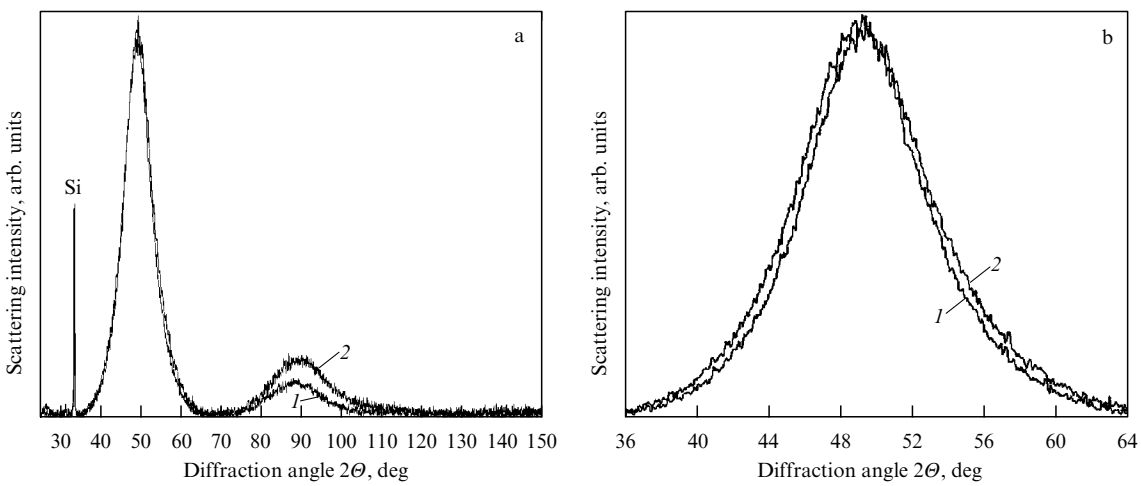

Figure 12. X-ray diffraction patterns of the amorphous alloy $Pd_{40}Ni_{40}P_{20}$ after rolling: (a) full angular range; and (b) region of the first maximum.

diffuse maximum in the directions along and across the tensile direction. The investigations were performed in situ in the process of deformation in the range of elastic stresses; the results obtained indicate an ellipsoidal shape of the first coordination shell.

Thus, the difference in the X-ray scattering by deformed samples observed in the $Pd_{40}Ni_{40}P_{20}$ alloy along and across the deformation direction, just as in [50–52], is caused by the different average interatomic spacings along and across the rolling direction in the deformed sample, i.e., by the ellipsoidal shape of the first coordination shell. However, in our studies, in contrast to [50–52], the samples were deformed plastically rather than elastically and the anisotropy of the structure was retained after the removal of the load; therefore, the factors responsible for the changes in the interatomic spacings can be more complex.

As is known, in the case of elastic deformation the elongation, according to Hook's law, depends linearly on stress. At greater loads, this dependence deviates from linear, in the amorphous alloys as well. If the shape of the sample is not restored completely after the removal of the load, i.e., if a so-called mechanical hysteresis loop appears, this indicates the occurrence of anelastic deformation of the material. The energy corresponding to the area of this loop is spent to displace atoms located in unstable positions. The magnitude of such displacements in amorphous alloys is, as a rule, larger by an order of magnitude than in crystalline alloys. It is assumed that the anelasticity of amorphous alloys is related to the magnitude of the free volume in their structure; namely, if the free volume is small, then the anelastic deformation is also small. Therefore, the anelasticity is related to the degree of relaxation of the structure, which leads to a decrease in the free volume. The anelastic deformation decreases after annealing, upon which a structural relaxation occurs [6].

Further plastic deformation of amorphous alloys is implemented via the formation and propagation of shear bands. The shear bands and slip lines were observed in a number of amorphous alloys. According to the literature data [54], the shear bands are oriented at an angle of $55 \pm 5°$ to the direction of deformation. One more specific feature of the plastic deformation of amorphous alloys is an increase in the concentration of the free volume in shear bands, i.e., an increase in the average spacing between the atoms. Upon annealing, the differences in the structure of the shear bands and the surrounding matrix can disappear completely or partly.

In addition to the deformation by the formation and propagation of shear bands, the amorphous alloy can also be deformed homogeneously (anelastically). The anelastic deformation during rolling leads to an anisotropic increase in the interatomic spacings and, consequently, to a change in the shape of the first coordination shell in the amorphous phase. An analysis performed has shown that the observed effect of the shift of diffuse peaks in X-ray diffraction patterns taken from the deformed samples along the rolling direction is related to the anelastic deformation of the main part of the sample. In full accordance with the suggested assumptions concerning the anelastic deformation as the factor responsible for the observed effect is the fact that, in the storage of a deformed sample (which is accompanied by relaxation of the structure), the distortion of the first coordination shell decreases.

Based on the investigations performed using X-ray radiations with different wavelengths [53], it was also established that the changes in the structure are more pronounced in the near-surface regions of the sample subjected to maximum deformation.

Characteristic changes in the structure during deformation were also noted when using the SAXS method. Thus, in the $Pd_{80}Si_{20}$ alloy the 20% deformation led to a noticeable increase in the intensity of the small-angle scattering [55], and in the $Fe_{40}Ni_{40}P_{14}B_6$ alloy [56] the available inhomogeneities with dimensions of 32 Å increased in size to 35 Å after 2 h annealing at 100 °C.

5.3 Evolution of the structure and properties under irradiation

Irradiation by neutrons or electrons leads to noticeable changes in the properties of amorphous alloys [57–60]. One of the most interesting effects is the recovery of the plasticity of the amorphous phase, which is related to the subdivision of the inhomogeneity regions that were formed after heat treatment and led to embrittlement. A feature common to all the alloys that have been studied is an increase in the electrical resistivity as the irradiation dose increases. After irradiation by thermal neutrons, regions of enhanced and reduced density (inhomogeneities of electron density) can arise in the amorphous phase. In some alloys, the neutron irradiation leads to a swelling of the amorphous phase. The irradiation of amorphous alloys in the general case leads to numerous changes in the structure of the amorphous phase, e.g. the formation of defects, and local changes in the density and chemical composition.

Thus, the irradiation of amorphous alloys can lead to both the formation of inhomogeneities and their disappearance. What is significant here is the fact that the irradiation changes the structure of the amorphous phase.

5.4 Evolution of the structure upon thermomagnetic treatment

It is well known that the use of thermomagnetic treatment can significantly change the properties of amorphous alloys. Thus, for example, the dependence of the coercive force of cobalt-based amorphous alloys on the annealing temperature is nonmonotonic, and the constant of induced magnetic anisotropy decreases upon annealing in a magnetic field [61]. Such changes in the properties should be caused by structural changes. The use of the SANS method also makes it possible to study structural changes under the effect of a magnetic field. As an example, in Ref. [62] the authors observed inhomogeneities in an amorphous alloy $Fe_{78}B_{12}Si_{10}$. These inhomogeneities (with a size of about 10^6 Å) have not been identified in [62]; they can be fluctuations of the density, chemical composition, spin density, etc. In the direction perpendicular to the ribbon plane all the inhomogeneities were distributed uniformly and had approximately the same size. After holding for 60 h in a magnetic field of 780 G, the inhomogeneities became elongated along the field.

6. Inhomogeneities arising during the production of amorphous phases

Immediately after preparation, an amorphous alloy can be non-single-phase and contain two or more amorphous phases. The data on the phase separation of amorphous alloys were obtained for $Pd_{74}Au_8Si_{18}$ [34], $Pd_{40.5}Ni_{40.5}P_{19}$ [63], $Be_{40}Ti_{24}Zr_{36}$ [64], and many other alloys. Let us consider several examples.

In the alloys of systems such as Al–Si–X and Al–Ge–X (X = Ti, Zr, V, W, Mn, Fe, Co, Ni, Cu, Cr, Nb, Mo) [65], a double halo in the XRD patterns was observed directly after preparation of the alloys; the scattering vectors of the two peaks in the $Al_{70}Si_{20}Ni_{10}$ alloy were 0.269 ± 0.003 and 0.322 ± 0.003 nm^{-1}. The XRD data coincided completely with the electron-diffraction data. From the analysis of the wave vectors of these peaks, the authors of [65] concluded that the peak located at smaller angles is due to preferential Al–Al neighbors, and the peak at larger angles is due to Si–(Al, X) or Ga–(Al, X) neighbors. According to the HREM data, the structure is characterized by an inhomogeneous distribution of atoms on a scale of 10 Å; the authors ascribed this to the insolubility of silicon and germanium in aluminum. The (Au–Pb–Pt)–(Pb–Sb) alloys [26] immediately after preparation in the amorphous state contained inhomogeneities of about 10 Å in size, spaced approximately 50 Å apart (in the crystallized regions, the size of the crystals was about 200 Å). Finally, phase separation was observed in the amorphous state in the Pd–Si–Sb system [66]. In some alloys of this system, the phase separation was observed within the amorphous state. Upon subsequent heating, the two arising amorphous phases crystallized independently of one another. The rate of crystallization of one of the phases is interface-limited.

The numerous examples given above indicate that, under the influence of various external factors, in the homogeneous amorphous structure diffusion processes can develop that lead to the formation of regions with different elemental compositions and/or different short-range orders, which, during subsequent crystallization, can exert the decisive effect on the arising crystalline structure and, naturally, on its properties.

7. Evolution of the amorphous-phase structure in the process of crystallization

The concentration redistribution of components in the amorphous phase can occur not only prior to the onset of crystallization, but also in the process of primary crystallization, when the composition of the arising crystals differs from the composition of the matrix, and the process of nucleation and growth of the crystals is accompanied by the diffusion of components from the front of a growing crystal into the bulk of the amorphous phase. It has been established that during primary crystallization, when the primary crystals precipitate from the amorphous phase, not only a monotonic variation of the composition of the amorphous phase, due to the precipitation of crystals of one of the components, but also more complex processes of phase separation can be observed.

As an example, we consider alloys of the Al–Ni–Y system. The nanocrystallization of aluminum-based amorphous alloys containing 10–15 at. % transition metal and 3–15 at. % rare-earth metal has been investigated in numerous studies, since these light alloys possess rather high strength. However, the processes that occur in the amorphous phase and the processes that precede or accompany nanocrystallization have been studied insufficiently. Meanwhile, it is precisely these processes that determine the morphology of nanocrystals, the fraction of the nanocrystalline phase, and the perfection of the structure of nanocrystals, which in the final account determine the strength properties of a material.

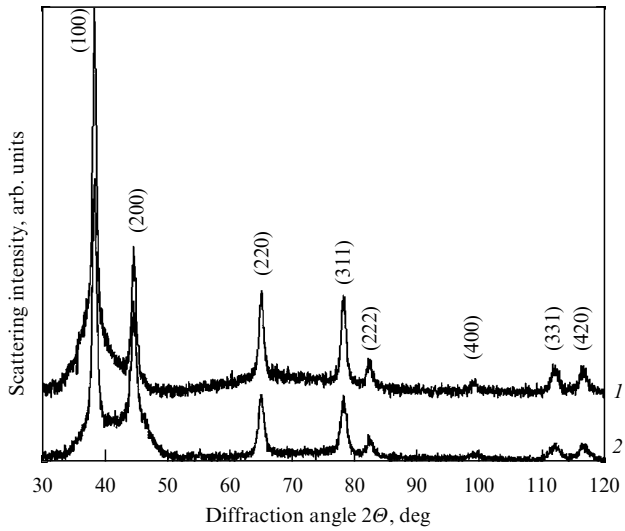

Figure 13. X-ray diffraction patterns of (*1*) $Al_{88}Ni_{10}Y_2$ and (*2*) $Al_{88}Ni_6Y_6$ amorphous alloys after the termination of the first stage of crystallization.

Let us consider two alloys containing the same amount of aluminum but characterized by different relationships between the nickel and yttrium contents, namely, $Al_{88}Ni_{10}Y_2$ (alloy 1) and $Al_{88}Ni_6Y_6$ (alloy 2) [67].

To study the effect of the elemental composition on the nanocrystallization processes, we investigated the structure of the samples in the same structural state, namely, when heated to a temperature at which the processes of primary crystallization are already completed. After the termination of the first stage of crystallization, the samples consist of precipitated nanocrystals of Al and the retained amorphous matrix (Fig. 13). The nanocrystals are single-component and represent precipitates of pure aluminum, which agrees with the phase diagrams, since neither nickel nor yttrium dissolve in aluminum [68].

Figures 14a and 14b display the resolutions of the heading parts of the spectra after the subtraction of the background. In the resolution of the peaks into the components, the parameters of the diffuse maxima of the initial amorphous samples have been taken into account. The positions of the diffuse peaks and their half-widths obtained for each alloy from the approximation of the curves from the initial amorphous samples were used in the resolutions of the corresponding peaks in the XRD patterns of the annealed samples presented in Fig. 14.

The results of the resolution show that, in spite of the similarity of the appearance of the experimental curves, the contributions to them from the diffraction and diffuse components (diffraction from the nanocrystalline phase and scattering by the amorphous phase, respectively) prove to be substantially different. In the alloy with a smaller content of yttrium (and higher content of nickel) (Fig. 14a), the diffuse halo from the amorphous phase is shifted to the region of larger angles compared to the positions of the halo from the initial amorphous phase.

The observed shift of the diffuse halo in the XRD patterns of the $Al_{88}Ni_{10}Y_2$ alloy toward larger angles indicates a decrease in the radius of the first coordination shell of the amorphous phase in the process of the formation and growth of nanocrystals. In the $Al_{88}Ni_6Y_6$ alloy with the greater concentration of yttrium (Fig. 14b), along with the main

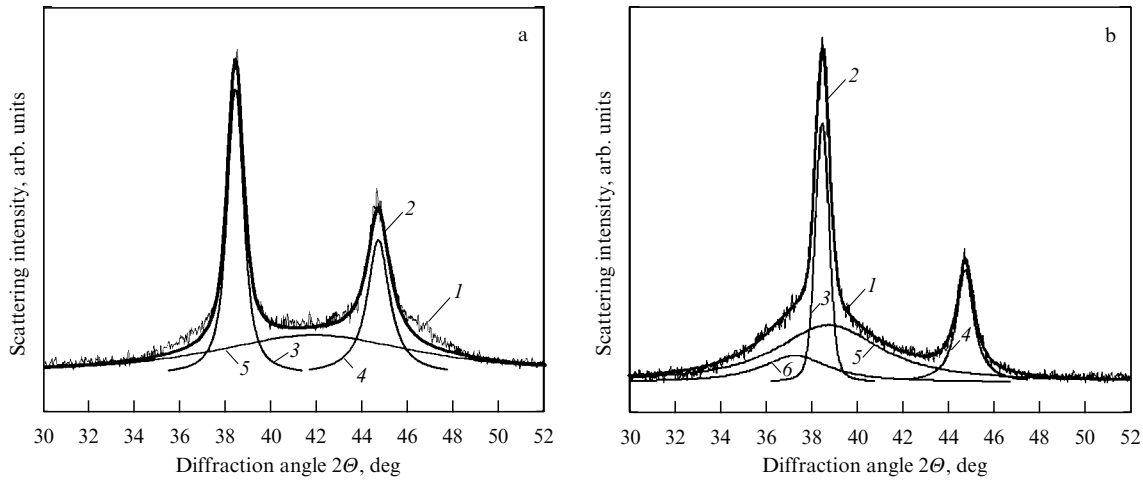

Figure 14. Initial regions of the X-ray diffraction patterns of the (a) $Al_{88}Ni_{10}Y_2$ and (b) $Al_{88}Ni_6Y_6$ amorphous alloys presented in Fig. 13: (*1*) experimental spectra and (*2–6*) resolution of the initial parts of the spectra; (*2*) total curve; (*3*, *4*) reflections of fcc Al; (*5*, *6*) scattering by the amorphous phase (phases).

maximum, an additional diffuse maximum on the side of smaller angles appears in the XRD pattern, and the main maximum is shifted somewhat toward larger angles. This indicates that in the amorphous phase regions of different (modified) chemical compositions appear; i.e. a mixture of two amorphous phases is formed. Since the additional diffuse maximum lies in the curve on the side of smaller angles, this means that the arising regions of the new amorphous phase are characterized by a greater radius of the first coordination shell.

As was already noted above, the changes in the positions of the diffuse maximum in the XRD patterns reflect the changes in the radius of the first coordination shell. Naturally, the radius of the first coordination shell depends on the dimensions of the atoms of the alloy components. In the system under consideration, the yttrium atoms are the largest (the radius of yttrium atoms is $R_Y = 0.181$ nm); the nickel atoms have the smallest radius ($R_{Ni} = 0.124$ nm); and the aluminum atoms have an intermediate size ($R_{Al} = 0.143$ nm). The shift of the halo in the XRD patterns toward greater angles in the $Al_{88}Ni_{10}Y_2$ alloy (with a greater content of nickel) means a decrease in the radius of the first coordination shell. Such a change can be related to an enrichment of the amorphous phase with nickel (and/or a depletion of yttrium) upon the precipitation of aluminum nanocrystals in the process of crystallization.

In the alloy containing 6 at.% Ni and 6 at.% Y, after the termination of primary crystallization an additional diffuse maximum appears on the side of smaller angles. The formation of an additional halo on the side of smaller angles indicates the appearance of a second amorphous phase with a greater radius of the first coordination shell. In this case, as was noted above, the main maximum shifts somewhat toward greater angles. The radii of the coordination shells for these two amorphous phases are 0.286 and 0.297 nm, respectively. It is obvious that the amorphous phase with the greater radius of the first coordination shell is enriched in yttrium. For the alloy with the smaller content of yttrium, the radius of the first coordination shell of the initial amorphous phase is 0.287 nm. This value is somewhat smaller than the radius of the first coordination shell of alloy 1, which is related to the different concentration of yttrium. After the termination of primary crystallization, the radius of the first coordination shell of the amorphous phase decreases to 0.267 nm; this indicates a greater concentration of nickel in the amorphous phase after the termination of the first stage of crystallization.

Thus, a relatively small change in the concentration of the rare-earth metal can lead to a significant change in the behavior of the amorphous phase before the onset of the second stage of crystallization. Until a certain 'critical' value of the concentration of the rare-earth metal is reached, the primary crystallization leads to merely a change in the composition of the initial amorphous matrix. As was already noted, the fraction of the nanocrystalline phase after the first stage of crystallization is usually no more than 25%. The estimates performed have shown that the composition of the amorphous phase in the alloy with 2 at.% yttrium changes from $Al_{88}Ni_{10}Y_2$ to $Al_{84}Ni_{13.3}Y_{2.7}$. Such a change in the composition of the amorphous alloy leads to the appearance of several amorphous phases with close values of the radius of the first coordination shell and to a decrease in the average radius of the first coordination shell. After an increase in the concentration of the rare-earth metal to above the critical value, a pronounced separation of the amorphous phase occurs. In the $Al_{88}Ni_6Y_6$ alloy, the precipitation of nanocrystals of aluminum according to the primary reaction should lead to a change in the composition of the amorphous phase from $Al_{88}Ni_6Y_6$ to $Al_{84}Ni_8Y_8$. The amorphous phase of such a composition appears to be unstable, which leads to its separation.

As was noted above, such a separation into several amorphous phases is observed quite frequently in amorphous alloys at the stages preceding crystallization [69–71]. A characteristic feature of such alloys is their complex composition and the presence of several phases in this concentration range in the equilibrium phase diagram.

Note that the two alloys under consideration differ strongly in the relationship of atomic concentrations Ni : Y (1 : 1 in the $Al_{88}Ni_6Y_6$ alloy and 5 : 1 in $Al_{88}Ni_{10}Y_2$). The equilibrium phase diagram of the Ni–Y system is quite rich in intermetallic compounds, starting with $Ni_{17}Y_2$ and ending at NiY_3 [68]; therefore, in the melt before quenching (and, correspondingly, in the amorphous alloy after quenching) clusters of different compositions and with different short-range orders can exist, which can favor separation.

The results of investigations obtained in Ref. [67] suggest that the nanocrystals in these alloys indeed nucleate via a heterogeneous mechanism and that the nucleation starts on sites depleted of the rare-earth component. These results represent an important contribution to the investigation of the processes of the formation of nanostructures aimed at the development of new materials with desired physical properties.

8. Phase separation in the amorphous phase under the impact of external factors

Thus, changes in the structure of an amorphous phase can occur upon heating, deformation, irradiation, and other exposures.

Deformation. As was already discussed, the deformation of the amorphous phase leads to changes in its structure — to the formation of shear bands or regions of reduced density and to changes in the interatomic spacings in both the shear bands and in the band-free part of the sample. In this case, the sample becomes 'two-phase' and consists of two amorphous phases of different densities. Depending on the deformation mode and on the elastic characteristics of the material, these changes can be developed to different extents and can be reversible or irreversible.

Heat Treatment. The changes in the structure of the amorphous phase depend substantially on the temperature range, i.e., on whether it is above or below the glass transition temperature T_g. In these temperature ranges, the physical properties of the material differ substantially. Above T_g, a noticeable decrease in the viscosity is observed, the contribution from elastic stresses becomes insignificant, the mobility of atoms grows substantially, and, naturally, the processes of diffusion mass transfer are facilitated. Above T_g, the diffusion processes proceed faster, and separation occurs to a greater extent.

Neutron Irradiation. Various changes in the structure can also be caused by irradiation. Depending on the irradiation parameters and the state of the material before irradiation, both the appearance and disappearance of inhomogeneities can occur upon irradiation.

But what factors are responsible for the separation of amorphous phases? As was said above, amorphous metallic glasses are formed upon rapid cooling of the melt. As is known, the structure of a liquid phase is by no means absolutely homogeneous. Numerous investigations that were conducted when studying both simple liquids and metallic melts have shown that the structure of melts is not homogeneous and depends on temperature. Near the melting point in the melts, regions exist with a certain type of short-range order (clusters). These clusters can be of different types and their number depends on both the number of alloy components and the complexity of the phase diagram, i.e., on the number of crystalline phases which can arise in a given system. This especially concerns the eutectic region, where even upon conventional slow solidification two or more crystalline phases are formed simultaneously. It is also known [72] that at a given composition the cluster structure of a liquid can change with changing temperature. Upon rapid cooling, when the structure of the melt is fixed at room temperature, the amorphous phase can also contain clusters of different types. The dependence of the structure of an amorphous phase on temperature (and, consequently, on the structure) of the liquid phase before cooling follows, for example, from the dependence of phase transformations that occur upon crystallization at the quenching temperature [73]. The existence of clusters of various types in the amorphous phase is also evidenced by the two values of the Curie temperature found in the Fe-based alloy [74], by observation [47] of the simultaneous existence of regions with different types of the short-range order, and by the changes in the type of short-range order with temperature within the amorphous state, which can even be reversible [48]. The short-range order also changes with a change in the alloy composition [38]; for example, in the amorphous phase with the composition $(Zr_{0.667}Ni_{0.333})_{1-x}B_x$ $(0 \leqslant x \leqslant 0.25)$, the short-range order changes at $x \approx 0.05$.

The decomposition of the amorphous phase can occur via different mechanisms. One of these is spinodal decomposition. This possibility was discussed, for example, in the investigation of the crystallization of Ag–Cu alloys [75]. However, the processes of spinodal decomposition can also take place prior to the beginning of crystallization. Investigations of the structural evolution in the amorphous phase of the Pd–Au–Si alloy and, in particular, the analysis of electron diffraction patterns taken at a temperature above the glass transition temperature have shown that in this alloy the spinodal decomposition of the amorphous phase occurs before the onset of crystallization [35].

Thus, regions with different types of short-range order and/or different compositions can exist in the amorphous phase immediately after preparation. For separation to start in the amorphous phase, these regions should start changing. This can occur if the free energy of the amorphous phase containing two types of clusters is less than that of the homogeneous amorphous phase. As is well known, the ability to form an amorphous phase is related to the existence of a 'deep' eutectic valley in the phase diagrams, which indicates a large negative heat of mixing [76]. However, systems exist which exhibit, at least in narrow concentration regions, a different behavior, i.e., a positive heat of mixing [77–79]. Consequently, a range of concentrations should exist in which the free energy of a mixture of two amorphous phases is less than that of a single amorphous phase. In this concentration range an amorphous phase decomposes into two amorphous phases. The process of decomposition of an amorphous phase (transition into a more equilibrium state) can be stimulated by various external factors.

9. Variation of properties in the process of amorphous-phase evolution

The physical properties of amorphous alloys are structure-sensitive and depend on external factors. The amorphous alloys are not thermally stable; therefore, subsequent annealing, even if it does not lead to crystallization, can cause changes in their structure, which can manifest themselves as an increase in the density and Young's modulus, the development of embrittlement, a decrease in the internal friction, changes in the magnetic properties, etc. Naturally, the processes of phase separation can also lead to noticeable changes in the properties of amorphous alloys. Let us consider some examples in addition to those discussed above.

9.1 Variation of the Curie temperature

In Ref. [80], it was established that, upon heating an amorphous alloy $Fe_{27}Ni_{63}P_{14}B_6$ in a temperature range

below the onset of crystallization, an increase is observed in the Curie temperature. Later, similar changes were also observed in some other alloys. The appearance of two Curie temperatures was also revealed when studying iron-based alloys [74], which indicates the coexistence of two amorphous phases.

9.2 Variation of plasticity

The plasticity of amorphous alloys decreases upon heating; the decrease can start, depending on the chemical composition, at temperatures sufficiently low compared to the crystallization temperature. The phenomenon of embrittlement of amorphous alloys was for the first time revealed in the $Fe_{40}Ni_{40}P_{14}B_6$ alloy and was ascribed to the presence of phosphorus, since it was found that the fracture surface is enriched in phosphorus [81]. However, Masumoto et al. [82] have shown that the Fe–Si–B alloys are also brittle, although they contain no phosphorus. The embrittlement is a distinctive property of amorphous alloys based on iron. Chen et al. [83, 84] revealed, while studying the dependence of embrittlement on the content of nonmetallic elements in such alloys, that the phenomenon of embrittlement is inherent in iron alloys containing both one and two metalloids. It can be supposed that the embrittlement of iron-based alloys containing two kinds of metalloids is caused by the fact that phase separation occurs easily upon heating these alloys.

10. Controlling the sample structure during crystallization

An important consequence of processes of phase separation within the amorphous state is the possibility of controlling the structure that is formed upon crystallization. We already noted above that the phase composition of the sample crystallized from an amorphous state can be different, depending on the conditions of crystallization [48]. It was also shown that quite different structures arise upon crystallization of amorphous alloys of the Ni–Mo–P and Ni–Mo–B systems upon heat treatment at temperatures above or below T_g, which is related to the different structure of the amorphous phase in these temperature regions. If the crystallization is preceded by a separation of the amorphous phase, a nanocrystalline structure can be obtained which cannot be produced upon conventional annealing (for example, in the Ni–Mo–B system [40]). As one more example, we can take the ferromagnetic alloy $Fe_{72}Al_5P_{10}Ga_2C_6B_4Si_1$ with good magnetic properties, in which the nanocrystalline structure is formed only above the glass transition temperature [85, 86]. The so-called SS phase can also be considered among such structures, which was revealed in the crystallization of some amorphous alloys on the basis of iron, cobalt, nickel, and palladium in 1976 [87], when the term 'nanostructure' did not yet exist.

Local changes in the composition of the alloy and the formation of regions with different compositions and, consequently, with different short-range order can be initiated by different treatments. By forming in the amorphous phase regions of different compositions and structures, crystalline samples with different phase compositions and morphologies of the crystalline phases can be obtained. For example, the annealing of amorphous alloys in a vacuum or in a special atmosphere can lead to a change in the elemental composition of the near-surface layer. Such investigations were performed on the amorphous alloy $Pd_{40}Ni_{40}P_{20}$, which usually crystallizes upon heating with the formation of several metastable crystalline phases [88] with crystallite sizes of ~ 200 nm, i.e., with the formation of a conventional crystalline rather than nanocrystalline structure. The typical structure of a crystallized sample is shown in Fig. 15.

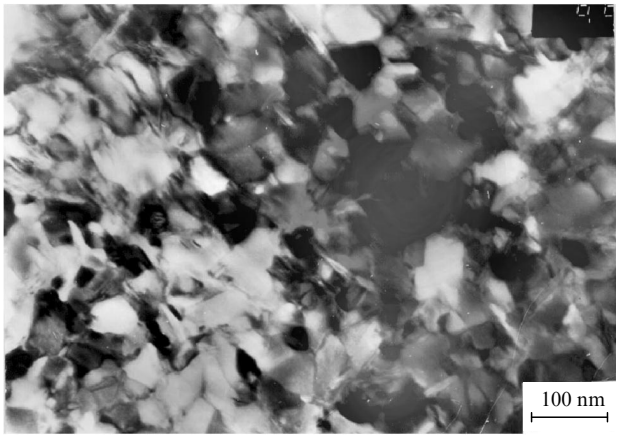

Figure 15. Microstructure of the crystallized $Pd_{40}Ni_{40}P_{20}$ alloy.

Figure 16. Layered structure of the near-surface region of the $Pd_{40}Ni_{40}P_{20}$ alloy.

The investigations performed in Ref. [89] have shown that in the near-surface region of the contact side of the ribbon (the ribbon side that was in contact with the substrate upon quenching), at the earlier stages of crystallization a layered structure consisting of crystalline and amorphous regions can form (Fig. 16). The formation of such a structure is due to the different chemical compositions of these regions and, consequently, due to their different thermal stability. The results obtained indicate a possible way to control structure — to change the composition in such a way that the mechanism of crystallization changes from eutectic to primary, since upon heating the amorphous phase the primary crystallization starts at temperatures that are lower than the eutectic temperature [90]. To strengthen the change in the composition of the near-surface region, samples of the alloy were held for a prolonged time at an enhanced temperature (583 K) under conditions of a dynamic vacuum. It has been shown by Auger electron spectroscopy that the near-surface layer is depleted of phosphorus because of its evaporation from the surface and insufficiently high rate of the diffusional supply

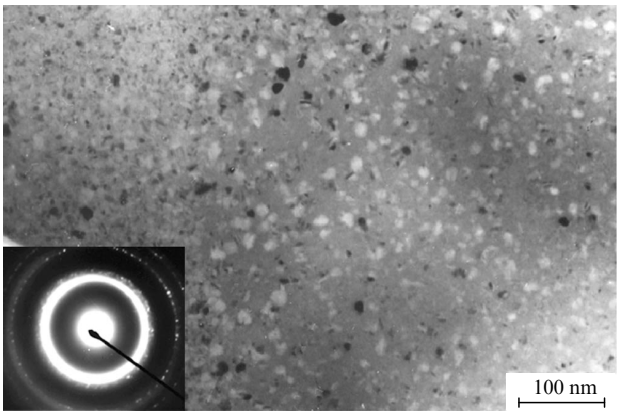

Figure 17. Microstructure of the near-surface region of the $Pd_{40}Ni_{40}P_{20}$ alloy after vacuum annealing.

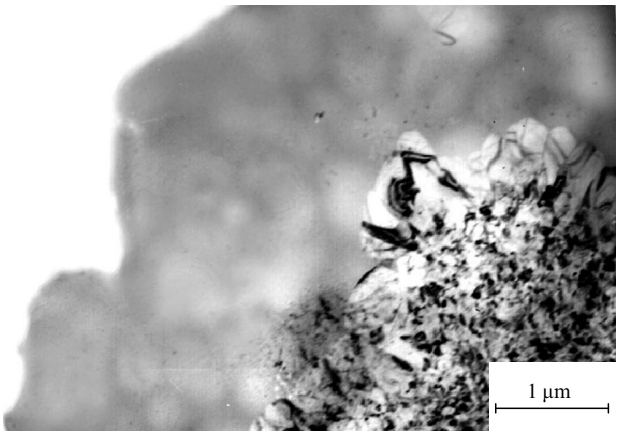

Figure 19. Microstructure of a partly in situ crystallized sample of the preliminarily annealed $Fe_{83}B_{10}P_7$ alloy.

of phosphorus from the bulk of the sample. The depth of the phosphorus-depleted region was about 50 nm. Since the concentration of phosphorus in the near-surface layers decreases during vacuum annealing to 8% and the composition became hypoeutectic, the crystallization of the amorphous phase with this modified composition occurred via the primary mechanism.

Thus, Aronin [89] obtained in the near-surface layer a nanocrystalline structure (Fig. 17) consisting of an amorphous phase and nanocrystalline nickel. As was already noted above, this change in the structure was achieved for the reason that, due to a change in the phosphorus concentration, the composition of the amorphous phase in the near-surface region changed from eutectic to hypoeutectic, which naturally led to a change in the mechanism of crystallization.

Ref. [91] can serve as a brilliant illustration of such an approach in which the authors have shown the possibility of controlling not only the amorphous structure but also the crystalline structure arising upon the crystallization of the amorphous phase. It was shown in [91] through the example of an Fe–B–P amorphous alloy that, by changing the conditions of heat treatment, an amorphous alloy with a crystalline surface can be obtained, or, if necessary, a crystalline alloy with an amorphous surface. The choice of the Fe–B–P alloy was related to the enhanced tendency of phosphorus to form segregates, which opened a way for the creation of a structure which substantially depends on the conditions of treatment. The use of various heat treatments made it possible to implement the process of crystallization, which started from the bulk of the sample rather than (the most common case) from the surface; the near-surface region remained amorphous in this case. Figures 18 and 19 display the structure of samples obtained in [91] under various heat-treatment conditions. Naturally, such samples should have different properties.

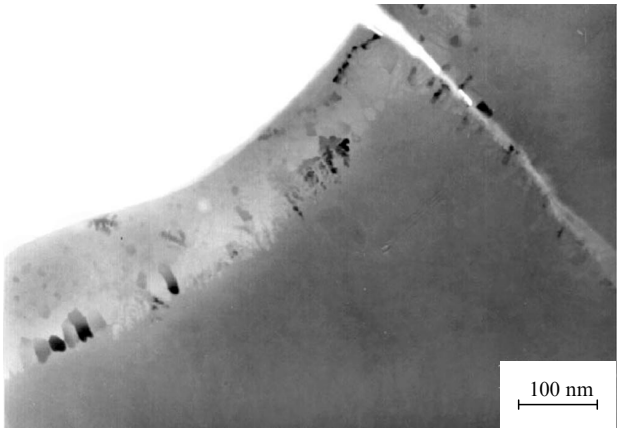

Figure 18. Microstructure of a partly in situ crystallized sample of the $Fe_{83}B_{10}P_7$ alloy.

The last alloy represents one more example which illustrates how the external stimulation of the phase separation of the amorphous alloy into regions with different compositions and different short-range orders makes it possible to produce structures of various types. The vacuum heat treatment induced composition changes in the near-surface layer, i.e., the appearance of differences between the structures of the amorphous phase in the near-surface zone and in the bulk, which led to different mechanisms of crystallization in these regions.

11. Conclusions

The results of investigations of the evolution of the structure in amorphous alloys have permitted researchers to make an important step both in the understanding of the structures of metallic glasses themselves and in controlling the structure of crystalline materials formed upon the decomposition of the amorphous phase. It has been established that the structure of the amorphous phase can change within the amorphous state prior to the onset of crystallization under the effects of heating, deformation, and irradiation. Numerous examples considered in this review indicate that quite various actions on a homogeneous amorphous structure can induce diffusion processes leading to the formation of regions with different elemental compositions and/or different short-range orders, which upon subsequent crystallization can exert a decisive effect on the arising structure and, naturally, on the properties of the resulting material. These processes differ most substantially in two temperature ranges: above and below the glass transition temperature. The mechanism of crystallization, phase composition, morphology, and size of crystals depend substantially on the conditions of treatment and, in particular, on the possibility of the formation of several amorphous phases, which can subsequently crystallize independently of one another. In alloys based on nickel, iron,

palladium, and some others, phase separation can occur, leading to the subsequent formation of a nanocrystalline structure. All these results make an important contribution to the investigations of the processes of the formation of nanostructures suitable for the creation of new materials with the required physical properties.

References

1. Duwez P, Willens R H, Klement W *J. Appl. Phys.* **31** 1136 (1960)
2. Miroshnichenko I S, Salli I V *Zavod. Lab.* (11) 1398 (1959) [*Ind. Lab.* **25** 1463 (1959)]
3. Yamamoto R, Matsuoka H, Doyama M *Phys. Lett. A* **64** 457 (1978)
4. Koizumi H, Ninomiya T *J. Phys. Soc. Jpn.* **44** 898 (1978)
5. Fukunaga T, Ichikawa T, Suzuki K, in *Amorphous Magnetism II* (Eds R A Levy, R Hasegawa) (New York: Plenum Press, 1977) p. 52
6. Suzuki K, Fujimori H, Hashimoto K (Eds) *Amorphous Metals* (London: Butterworths, 1983) [Translated into Russian (Moscow: Metallurgiya, 1987)]
7. He Y, Poon S J, Shiflet G J *Science* **241** 1640 (1988)
8. Gleiter H *Prog. Mater. Sci.* **33** 223 (1989)
9. Birringer R *Mater. Sci. Eng. A* **117** 33 (1989)
10. Abrosimova G E et al. *Nanostructured Mater.* **12** 617 (1999)
11. Inoue A et al. *Mater. Sci. Eng. A* **179 – 180** 649 (1994)
12. Kim Y-H, Inoue A, Masumoto T *Mater. Trans. JIM* **32** 331 (1991)
13. Cahn R W, Haasen P (Eds) *Physical Metallurgy* Vol. 2 (Amsterdam: North-Holland, 1983) [Translated into Russian: Vol. 2 (Moscow: Metallurgiya, 1987)]
14. Uhlmann D R *J. Non-Cryst. Solids* **7** 337 (1972)
15. Davies H A *Phys. Chem. Glasses* **17** 159 (1976)
16. Nagel S R, Tauc J *Solid State Commun.* **22** 129 (1977)
17. Ichikawa T *Phys. Status Solidi A* **29** 293 (1975)
18. Yamamoto R, Matsuoka H, Doyama M *J. Phys. F* **7** L243 (1977)
19. Egami T, Vitek V, Srolovitz D, in *Proc. 4th Int. Conf. on Rapidly Quenched Metals, Sendai, 1981* (Eds T Masumoto, K Suzuki) (Sendai: Institute of Metals Japan, 1982) p. 2
20. Shiga M *J. Phys. Soc. Jpn.* **50** 2573 (1981)
21. Hiroyoshi H, Fukamichi K *J. Appl. Phys.* **53** 2226 (1982)
22. Egami T *Mater. Res. Bull.* **13** 557 (1978)
23. Masumoto T, Maddin R *Mater. Sci. Eng.* **19** 1 (1975)
24. Chen H S *Rep. Prog. Phys.* **43** 353 (1980)
25. Skryshevskii A F *Strukturnyi Analiz Zhidkostei i Amorfnykh Tel* (Structural Analysis of Liquids and Amorphous Materials) (Moscow: Vyssh. Shkola, 1980)
26. Yavari A R *Acta Metallurg.* **36** 1863 (1988)
27. Kraus W, Nolze G *J. Appl. Cryst.* **29** 301 (1996)
28. Guinier A *Théorie et technique de la radiocristallographie* (Paris: Dunod, 1956)
29. Huang S *Structure and Structure Analysis of Amorphous Materials* (Oxford: Clarendon Press, 1984)
30. Zhang X Y et al. *J. Appl. Phys.* **84** 1918 (1998)
31. Gloriant T et al. *Mater. Sci. Forum* **343 – 346** 365 (2000)
32. Abrosimova G E, Aronin A S, Kholstinina N N *Fiz. Tverd. Tela* **52** 417 (2010) [*Phys. Solid State* **52** 445 (2010)]
33. Svergun D I, Feigin L A *Rentgenovskoe i Neitronnoe Malouglovoe Rasseyanie* (Structure Analysis by Small-Angle X-ray and Neutron Scattering) (Moscow: Nauka, 1986) [Translated into English (New York: Plenum Press, 1987)]
34. Chou C-P P, Turnbull D *J. Non-Cryst. Solids* **17** 169 (1975)
35. Chen H S, Turnbull D *Acta Metallurg.* **17** 1021 (1969)
36. Mehra M, Schulz R, Johnson W L *J. Non-Cryst. Solids* **61 – 62** 859 (1984)
37. Nagarajan T et al. *Hyperfine Interact.* **34** 491 (1987)
38. Mak A, Samwer K, Johnson W L *Phys. Lett. A* **98** 353 (1983)
39. Abrosimova G E et al. *J. Magn. Magn. Mater.* **203** 169 (1999)
40. Abrosimova G, Aronin A, Ignatieva E *Mater. Sci. Eng. A* **449 – 451** 485 (2007)
41. Terauchi H et al. *J. Phys. Soc. Jpn.* **52** 3454 (1983)
42. Osamura K, Ochiai S, Takayama S *J. Mater. Sci.* **19** 1917 (1984)
43. Abrosimova G E, Aronin A S *Fiz. Tverd. Tela* **40** 1769 (1998) [*Phys. Solid State* **40** 1603 (1998)]
44. Osamura K et al. *Colloid. Polymer Sci.* **259** 677 (1981)
45. Naudon A, Flank A M *J. Non-Cryst. Solids* **61 – 62** 355 (1984)
46. Abrosimova G E et al. *Fiz. Met. Metalloved.* **62** 496 (1986)
47. Pokatilov V S *Dokl. Akad. Nauk SSSR* **275** 79 (1984) [*Sov. Phys. Dokl.* **29** 234 (1984)]
48. Abrosimova G E, Aronin A S *Int. J. Rapid Solidificat.* **6** 29 (1991)
49. Pampillo C A *J. Mater. Sci.* **10** 1194 (1975)
50. Wang X D et al. *Appl. Phys. Lett.* **91** 081913 (2007)
51. Stoica M et al. *J. Appl. Phys.* **104** 013522 (2008)
52. Wang X D et al. *Appl. Phys. Lett.* **94** 011911 (2009)
53. Abrosimova G E et al. *Fiz. Tverd. Tela* **52** 1763 (2010) [*Phys. Solid State* **52** 1892 (2010)]
54. Herman H (Ed.) *Ultrarapid Quenching of Liquid Alloys* (Treatise on Materials Science and Technology, Vol. 20) (New York: Academic Press, 1981) [Translated into Russian (Moscow: Metallurgiya, 1986)]
55. Suzuki C K, Doi K, Kohra K *Jpn. J. Appl. Phys.* **20** L271 (1981)
56. Walter J L, Legrand D G, Luborsky F E *Mater. Sci. Eng.* **29** 161 (1977)
57. Doi K, Ayano T, Kawamura K *J. Non-Cryst. Solids* **34** 405 (1979)
58. Gerling R, Wagner R *Scripta Metallurg.* **16** 963 (1982)
59. Gerling R, Wagner R *J. Nucl. Mater.* **107** 311 (1982)
60. Doi K, Kayano H, Masumoto T *J. Appl. Cryst.* **11** 605 (1978)
61. Fujimori H et al., in *Rapidly Quenched Metals III* Vol. 2 (Ed. B Cantor) (London: Metals Society, 1978) p. 232
62. Tomimitsu H et al. *J. Non-Cryst. Solids* **88** 388 (1986)
63. Chen H S *Mater Sci. Eng.* **23** 151 (1976)
64. Tanner L E, Ray R *Scripta Metallurg.* **14** 657 (1980)
65. Inoue A et al. *J. Mater. Sci. Lett.* **6** 94 (1987)
66. Marcus M A *J. Non-Cryst. Solids* **30** 317 (1979)
67. Abrosimova G E, Aronin A S *Fiz. Tverd. Tela* **51** 1665 (2009) [*Phys. Solid State* **51** 1765 (2009)]
68. Elliot R P (Ed.) *Constitution of Binary Alloys. First Supplement* (New York: McGraw-Hill, 1965) p. 472
69. Yavari A R et al. *Phys. Rev. B* **37** 7759 (1988)
70. Inoue A et al. *J. Mater. Sci. Lett.* **6** 194 (1987)
71. Abrosimova G E, Aronin A S, Voropaeva L V *Metallofizika* **11** (3) 102 (1989)
72. Popel P S, Sidorov V E *Mater. Sci. Eng. A* **226** 237 (1997)
73. Abrosimova G E et al. *Scripta Metallurg.* **14** 967 (1980)
74. Abrosimova G E, Serebryakov A V, Sokolovskaya Zh D, in *IV Vsesoyuz. Seminar po Amorfnomu Magnetizmu, Vladivostok, 10 – 13 Oktyabrya 1986 g., Tezisy Dokladov* (IV All-Union Seminar on Amorphous Magnetism, Vladivostok, October 10 – 13, 1986, Abstracts of Talks) (Krasnoyarsk: Inst. Fiziki, Sib Otd. Akad. Nauk SSSR, 1986) p. 134
75. Stoering R, Conrad H *Acta Metallurg.* **17** 933 (1969)
76. Marcus M, Turnbull D *Mater Sci. Eng.* **23** 211 (1976)
77. Köster U, Herold U, in *Glassy Metals* Vol. 1 *Ionic Structure, Electronic Transport, and Crystallization* (Eds H-J Güntherodt, H Beck) (New York: Springer-Verlag, 1982) p. 376
78. Oh J C et al. *Scripta Mater.* **53** 165 (2005)
79. Tian N et al. *Trans. JIM* **46** 2880 (2006)
80. Liebermann H H et al. *IEEE Trans. Magn.* **13** 1541 (1977)
81. Walter J L, Bacon F, Luborsky F E *Mater. Sci. Eng.* **24** 239 (1976)
82. Waseda Y, Okazaki H, Masumoto T, in *The Structure of Non-Crystalline Materials* (Ed. P H Gaskell) (London: Taylor and Francis, 1977) p. 95
83. Chen H S *Mater. Sci. Eng.* **26** 79 (1976)
84. Naka M, Masumoto T, Chen H S *J. Physique Colloques* **41** C8-839 (1980)
85. Abrosimova G E et al. *Fiz. Tverd. Tela* **46** 858 (2004) [*Phys. Solid State* **46** 885 (2004)]
86. Abrosimova G E et al. *Fiz. Tverd. Tela* **46** 2158 (2004) [*Phys. Solid State* **46** 2232 (2004)]
87. Masumoto T et al., Sci. Rep. RITU No. 26 (1976) p. 26
88. Aronin A et al. *J. Non-Cryst. Solids* **208** 139 (1996)
89. Aronin A *Nanostruct. Mater.* **8** 171 (1997)
90. Luborsky F E (Ed.) *Amorphous Metallic Alloys* (London: Butterworth-Heinemann, 1983) [Translated into Russian (Moscow: Metallurgiya, 1987)]
91. Aronin A S, Ivanov S A, Yakshin A E *Fiz. Tverd. Tela* **33** 2527 (1991) [*Phys. Solid State* **33** 1427 (1991)]
92. Klement W (Jr), Willens R H, Duwez P *Nature* **187** 809 (1960)